Simulating 0.4–2.5 GHz Brightness Temperatures of the Ross Ice Shelf, Antarctica

M. Brogioni, *Member, IEEE*, K. C. Jezek, Joel T. Johnson, *Fellow, IEEE*, M. Leduc-Leballeur, C. Yardim, *Member, IEEE*, L. Tsang, *Life Fellow, IEEE*, S. Wang, and G. Macelloni, *Senior Member, IEEE*

***Abstract*— Ice shelves are important parts of the cryosphere that influence ice sheet dynamics and mass loss. The internal temperatures of ice shelves are currently known only from a few borehole sites or from glaciological models. Microwave radiometry in the 0.4–2.5 GHz range is capable of receiving thermal emissions from deep within an ice shelf and thereby providing information on internal temperatures. This letter reports modeling studies of the brightness temperature of the Ross Ice Shelf (RIS) from 0.4 to 2.5 GHz that provide insight into the potential of microwave radiometers for measuring ice shelf internal properties.**

***Index Terms*— Antarctica, ice shelf, low frequency, microwave radiometry, modeling.**

I. Introduction

ICE shelves are the floating extension of inland glaciers that play a pivotal role in polar environments by stabilizing ice sheet grounding lines and constraining ice sheet discharge. The retreat of ice shelves is particularly important because ice shelves modulate land ice contributions to global sea level rise via their buttressing effect [1]. If surface melt occurs, water infiltration within ice shelf crevasses can cause hydrofracturing and trigger dynamic instabilities that lead to grounding line retreat [2]. Several geophysical campaigns such as the recent ROSETTA-Ice [3] have surveyed the Ross Ice Shelf (RIS), revealing ice flow directions, ice shelf mass balance, near-surface temperature, and providing evidence of past instabilities in West Antarctic ice sheet flow (e.g., [4]). However, many other RIS parameters remain poorly known, e.g., marine ice accretion regions and internal temperatures, with borehole parameters available only at the RIS Project (RISP) station J-9 [5] and the Little America V (LAV) site [6], [7], see Fig. 1. Detailed knowledge of the 3-D temperature field within ice shelves is required to improve ice shelf flow models. Microwave radiometry at 1.4 GHz has recently proven successful in estimating inland ice sheet internal temperatures up to 1 km depth [10]. Ultrawideband radiometry over the 0.5–2 GHz range further extends this capability to the entire ice sheet depth [11], representing a significant potential for bridging existing knowledge gaps in ice rheology [12], [13], [14]. Because sub-2 GHz brightness temperature measurements for the RIS are available currently only at 1.4 GHz, this potential has yet to be tested on ice shelves, but a detailed analysis of relationships between RIS geophysical parameters and 1.4 GHz brightness temperature (Tb) observations is provided in [16]. The present work focuses on modeling the RIS Tb for the frequency range of 0.4–2.5 GHz at the two test sites where englacial thermodynamic and geophysical parameters are available. The objective is to examine and interpret the Tb spectrum focusing on the penetration depth of microwave emissions from ice shelf. This analysis aims to inform the planning of future surveys and satellite mission proposals (e.g., Cryorad to ESA [16] and PolarRad to NASA [17]) and to contribute to geophysical parameter retrievals.

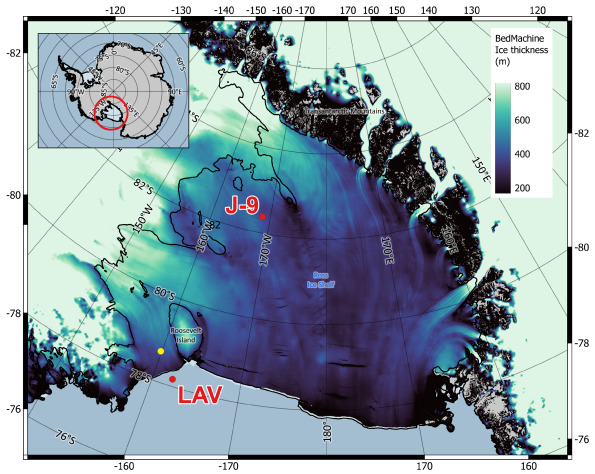

Fig. 1. RIS ice thickness map [8], [9] and the location of J-9 and LAV sites (red dots). Yellow dot is the site used in lieu of LAV.

II. Test Sites

The RIS is a tabular mass of "permanent" floating ice with a thickness ranging from 1200 m along the inland grounding

Manuscript received 22 December 2023; revised 14 February 2024; accepted 14 February 2024. Date of publication 22 February 2024; date of current version 1 March 2024. *(Corresponding author: M. Brogioni.)*

M. Brogioni, M. Leduc-Leballeur, and G. Macelloni are with the Institute of Applied Physics "N. Carrara," National Research Council, 50019 Sesto Fiorentino, Italy (e-mail: marco.brogioni@cnr.it).

K. C. Jezek is with the Byrd Polar and Climate Research Center, The Ohio State University, Columbus, OH 43210 USA (e-mail: jezek15@gmail.com).

Joel T. Johnson and C. Yardim are with the ElectroScience Laboratory, The Ohio State University, Columbus, OH 43210 USA (e-mail: johnson.1374@osu.edu).

L. Tsang is with the Radiation Laboratory, Department of Electrical Engineering and Computer Science, University of Michigan, Ann Arbor, MI 48109 USA (e-mail: leutsang@umich.edu).

S. Wang is with the Department of Geography and Earth and Environmental Systems Institute, Pennsylvania State University, University Park, PA 16802 USA (e-mail: skw5660@psu.edu).

Digital Object Identifier 10.1109/LGRS.2024.3368613

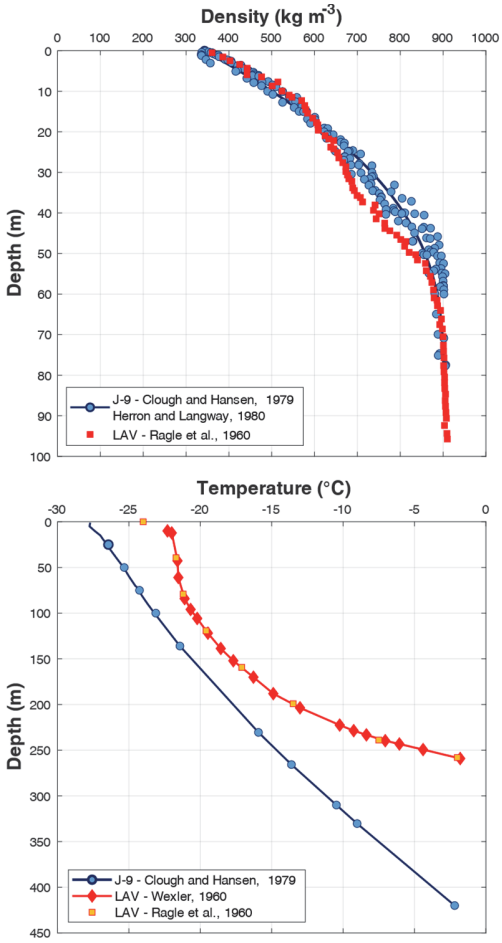

Fig. 2. Density (top) and temperature (bottom) profiles at J-9 (blue) and LAV (red) from in situ measurements [5], [7], [23].

line to less than 300 m closer to the calving front [9] (Fig. 1). In contrast to sea ice, which consists of a mix of ice, air, and small percentage of brine, the RIS is mainly composed of "pure" ice either transported from the Antarctic East and West ice sheets or deposited as annual snow accumulation. With an area of ~500 000 km^2, the RIS is the largest Antarctic ice shelf [18]. Despite its size, its englacial parameters have been collected only at two borehole sites: J-9 and LAV (Fig. 2). The ice shelf is approximately in mass balance and the fundamental characteristics of the ice shelf's strain field have not changed substantially since RIS Glaciological and Geophysical Survey—RIGGS, allowing for the use of past datasets in the current analysis [3].

A. RISP J-9

The J-9 site is located at (82.375 S; 168.618 W) in the interior of the RIS. The borehole was drilled in 1976 during the RIS Project [5] and the surrounding area was surveyed during the 1973–1978 RIS Geophysical and Glaciological Survey (RIGGS) in order to study the geophysical properties of the internal part of the ice shelf [4]. The ice shelf at J-9 is 420 m thick with a 6-m bottom accretion of marine ice (2–4 ppt saline concentration [19]). In situ density measurements show a firn-to-ice transition at about 60 m depth (see [20], [21], Fig. 2 (top)]. Englacial temperature at J-9 [5] shows a profile that increases almost linearly [Fig. 2 (bottom)]. Large bottom crevasses are also a notable feature of the ice shelf in the vicinity of J-9 [22]. These crevasses extend upward to 120 m into the ice shelf, are spaced between 1 and 2 km, and trend roughly normal to the flow direction. A shallower (50–70 m) second set of crevasses is offset by 60°. The crevasses are presumed to be seawater filled [22].

B. Little America V

Once located at (78.167 S; 162.217 W) near Roosvelt Island, LAV was one of the test sites of Operation Deep Freeze. The borehole was drilled during the 1958 International Polar Year close to the ice shelf edge (less than 10 km) and the facility was lost after a calving event. The ice shelf thickness at the drill site was 258 m [7]. In contrast to J-9, accreted basal marine ice is absent indicating melting at the bottom of the ice shelf [23]. The LAV surface firn was about 60 m thick with layering characteristics similar to those at J-9 [7] although a small inflection is observed between 20 and 50 m deep. The temperature profile is also monotonic with depth although more curved than at J-9 due to upstream advection [23].

III. Brightness Temperature Modeling

Microwave emission of snow/firn and glacier ice from 0.4 to 2.5 GHz is characterized by a low extinction coefficient and an almost complete lack of volume scattering, simplifying radiative transfer modeling. As in [10] and [25], the dense medium radiative transfer theory in its multilayer formulation (DMRT-ML, [26], [27]) has been used to estimate the RIS electromagnetic signatures via a Monte Carlo method. Inputs to the model come from in situ measurements.

An important parameter for the microwave emission process is the vertical density profile of the ice shelf. Due to geophysical processes (e.g., water vapor transport in the snow and firn densification due to the burden of the overlying layers), the inhomogeneous ice density in the upper 50 m causes reflection effects that strongly affect brightness temperatures [10]. The layering profile was computed based on a simple mass continuity model [28] where the surface density was set to 340 kg m^{-3} [20] and the surface accumulation to 9 cm yr^{-1} of water equivalent [21] (work [29] reports a similar value of 7.5 cm yr^{-1}). Given that layering affects the shallow part of the ice shelf and that the superficial temperature shows only slight spatial variations [15], the J-9 experimental density profile (Fig. 2) with superimposed random variations is used for both test sites. Density fluctuations from the average profile $\bar{\rho}(z)$ are modeled as damped Gaussian noise

$$\rho(z) = \bar{\rho}(z) + G(\mu = 0, \sigma = 50) * \exp(-0.05 * z)$$

where G indicates a Gaussian random variable with zero mean and standard deviation $\sigma = 50$ kg m^{-3} as verified with the borehole density measurements at LAV and J-9. The layer thickness was also perturbed using a Gaussian noise

$$d(z_n) = \bar{d}(z_n) + G(\mu = 0, \sigma = 0.1 * (\bar{d}(z_n) - \bar{d}(z_{n-1})))$$

where $\bar{d}(z_n)$ indicates the mean layer thickness coming from the mass continuity model [28]. Given the absence of detailed

in situ measurements on spatial correlations in the density and thickness fluctuations, no correlation between layer parameters is assumed. As expected (e.g., [25]), simulations (not presented here) showed that the layer thickness fluctuations impacted the mean over frequency of the Tb spectrum but not its frequency dependence; the mean layer thickness value that provides a minimum difference between simulated and measured Tb at 1.4 GHz, horizontal polarization, is used. The permittivities of pure and accreted ice were computed using the models of [30] and [31], respectively. A Monte Carlo simulation of brightness temperatures was performed over 100 realizations of the random density and thickness profiles for each of the test sites. In the following, we present the Tb as mean and standard deviation values. Model simulations were then compared with 2021 year average measurements from NASA's Soil Moisture Active Passive (SMAP) (reprocessed L1B data, 3-km ground resolution [32], [33]) and ESA's Soil Moisture Ocean Salinity (SMOS) missions (40-km ground resolution [34]) at 1.4 GHz, the only frequency currently available from 0.4 to 2.5 GHz for the RIS. Because the ice front retreated south of the LAV geographic location in 1987, SMAP measurements from a location near the original site were used under the assumption that sites in the area at a comparable distance from the RIS seaward edge have similar glaciological characteristics. The selected EASE2 grid pixel is centered on (78.694 S; 159.875 W, yellow dot in Fig. 1), in a homogeneous region that excludes nearby Roosvelt Island and the ice shelf terminus, and shows minimal variations in measured Tb's from summer to winter, thus ensuring minimal land/sea contamination.

IV. Results

At J-9, Tb simulations were performed by either neglecting the accretion layer or by modeling it as multiyear sea ice because of its low salinity [31]. Fig. 3 (top) presents Tb simulations at a 40° incidence angle for J-9 as a function of frequency, along with SMAP observations at 1.4 GHz. For both horizontal (H) and vertical (V) polarizations, the modeled Tb difference between the two bottom scenarios is greater at lower frequencies: at 0.4 GHz, the H pol Tb difference with and without marine ice is about 8 K, and at V pol, it is almost 15 K. At 1.4 GHz, the two scenarios yield smaller differences (3 K in V pol and 0.7 K in H pol). For H pol, in the case with bottom marine ice, SMAP observations and simulations show good agreement due to the layer thickness fitting. The V pol SMAP Tb lies between the curves of the two scenarios. In both polarizations, given the uncertainties of SMAP data (year 2021 time series standard deviation 0.8 K at V pol and 1.8 K at H pol) and the simulations (1.3 K as resulted from the Monte Carlo analysis), it is not possible to clearly distinguish the sea/ice interface condition. At the LAV site [Fig. 3 (bottom)], modeled spectra show an increasing trend in the frequency of greater dynamic range than that for J-9 (26 and 9 K at V pol) due to the shallower ice and associated attenuation of sea emissions at the LAV site. The comparison with SMAP shows an overestimation of 3 K for V pol and a good match for H pol.

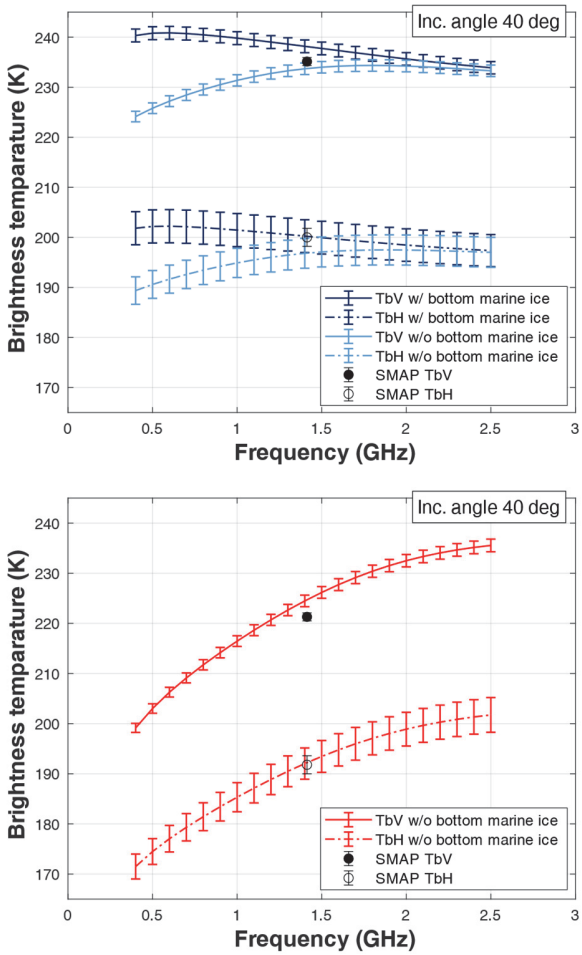

Fig. 3. Modeled Tb spectra at 40° at J-9 (top) and LAV (bottom) with (darker colors) and without (lighter colors) marine ice accretion. SMAP observations are shown as dots. Error bars indicate the standard deviation of the simulations and measurements.

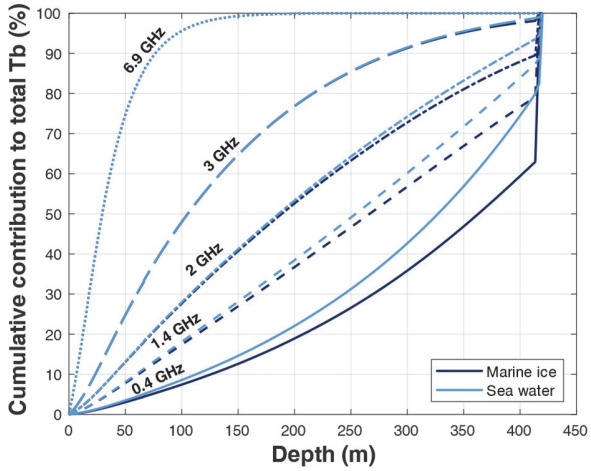

Fig. 4. Cumulative emission (reported as a percentage of the total Tb) estimated for J-9 site at 0.4 (P-band, continuous line), 1.4 (L-band, dashed), 2.0 and 3.0 (S-band, dot dashed and long dashed), and 6.9 (C-band, dotted) GHz.

To investigate the contribution of emissions from various depths, the cumulative layer contribution (beginning at the surface) to the total brightness temperature was analyzed at J-9 for both bottom scenarios (Fig. 4). At 0.4 GHz, emissions are significant from all depths within the ice shelf base

depending on the presence or absence of marine ice at the bottom. This is likely because the pure ice/water interface has a larger reflection coefficient than the pure ice/marine ice boundary. This means that the pure ice/water boundary more efficiently reflects the downward emission from the ice. Also, because of the strong attenuation of the 6-m marine ice, the emission contribution of the underlying seawater is obscured and the condition of a semi-infinite medium can be assumed. At 1.4 GHz, the results are similar, but the sub-shelf percentage is reduced to 21% and 11% with and without marine ice, respectively, and the linear trend suggests that layers within the ice shelf contribute approximately equally. At 2 GHz, the contributions of the deep layers continue to decrease, and the basal fraction reduces to 10% and 6%. Finally, at 3 GHz, emissions arise almost entirely from the upper layers of the pure ice, with no contribution from the lower regions. The results at 6.9 GHz (added because is the second lowest frequency currently available for spaceborne radiometers, e.g., JAXA AMSR2 and future ESA CIMR) highlight the limited penetration at this frequency: only the top 150 m contributes to the emission. The resulting effective penetration depths (the depth at which the medium above emits $1 - e^{-1}$ of the total Tb [35]) at 0.4, 1.4, 2, 3, and 6.9 GHz are 413, 332, 250, 145, and 38 m, respectively, in the case of bottom marine ice, and 369, 313, 245, 145, and 39 m without. This points out that the penetration depth (commonly defined for a homogeneous semi-infinite medium) is influenced by the overall structure of the medium, including its interface reflections, particularly at very low frequencies (<1.4 GHz). In comparison, at Dome C (75.1°S; 123.4°E) over the Antarctic Plateau, the penetration depth at 1.4 GHz is estimated to be about 1000 m [25], much deeper than that apparent in Fig. 4. This difference is related to the increased losses generated by the warmer ice temperature of the RIS [15]. This has major implications in using low-frequency radiometers for cryospheric studies since the ice temperature not only directly impacts brightness temperatures but also modulates the ice thickness contributing to the total emission.

V. Discussion

The results shown indicate that Tb at low frequencies (<1.4 GHz) can be sensitive to the basal conditions of Antarctic ice shelves and that wideband low-frequency radiometry can be used to infer the presence or absence of bottom marine ice accretion. At LAV, simulations compare favorably with SMAP and are consistent with the observation that melt is occurring at the ice shelf base (basal marine ice would increase the Tb even further). At J-9, where marine ice is expected, the model results support the hypothesis that the 0.4–2.5 GHz brightness temperature spectra can differentiate between basal conditions. Simulations shown in Fig. 5 for nadiral observations as proposed for future satellite missions [16] support the use of ultrawideband radiometry to infer the basal conditions of cold ice shelves and at locations outside the crevassed shear zones and firn aquifers. The nadiral spectra in Fig. 5 are as expected nearly the average of the V and H data in Fig. 3. The Tb difference between the marine ice and marine ice-free cases is similar for both nadir and oblique viewing angles (about 15 K at maximum). Thus, the sensitivity to the two

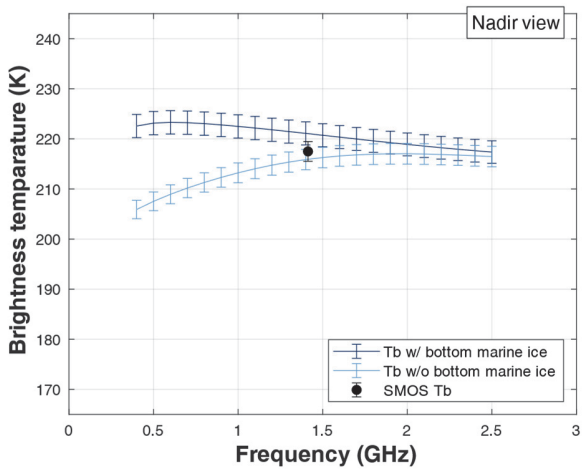

Fig. 5. Modeled brightness temperature spectra of the RIS at J-9 with (blue) and without (light blue) marine ice accretion at nadir. Black dot indicates SMOS averaged V and H pols Tb at 20° for 2021. Error bars indicate the standard deviation of the simulations and measurements.

basal scenarios is about the same for the nadir configuration. Existing low-frequency (i.e., 1.4 GHz) satellite radiometers are not sensitive enough to detect the presence or absence of marine ice, especially when measurement uncertainties are considered (Figs. 3 (top) and 5). There are several possible reasons why marine ice is not strongly influencing 1.4 GHz emissions. First, the actual penetration depth may be less than that assumed in this analysis. In [15], it is shown that correlations between SMAP 1.4 GHz Tb and ice thickness over RIS decrease for thicknesses greater than 400 m and become insignificant for thickness 700 m or more. This suggests that over the RIS, Tb at 1.4 GHz is sensitive to about the first 400–500 m of ice and not very sensitive to the properties of deeper ice in the column. This is consistent with estimates of the temperature-dependent absorption coefficient, which increases with temperature [30]. A second possibility is the impact of bottom crevasses on Tb. As described earlier, the largest crevasses extend about 120 m from the base. They appear roughly triangular with a basal width of about 130 m and can be several kilometers long (a maximum length was not reported in in situ observations). These structures increase the area available for emission, especially in the upper portions of the shelf where cooler physical temperatures create cooler Tb across the entire spectrum. On the other hand, crevasses also shadow emissions from warmer, deeper portions of the shelf that are located away from the viewing geometry and thereby may reduce emissions from basal ice. Moreover, because the base of the ice shelf is effectively a 2-D pattern of marine ice and water, the average Tb might be expected to be cooled for nadiral observations. The regular orientation of the crevasses may also lead to an azimuthal variation in Tb, but such an effect has yet to be investigated. These questions remain to be addressed in future work given the limitations of the model (only planar interfaces) used. Also, future theoretical modeling can consider the horizontal correlation lengths of density fluctuations [36] to take into account angular and polarization coupling in the brightness temperatures of SMAP.

VI. Conclusion

The modeling studies reported confirm the potential of microwave radiometry from 0.4 to 2.5 GHz for probing the

interior properties of ice shelves. The reasonable agreement of model predictions and SMAP and SMOS measurements supports the conclusion that microwave 1.4 GHz emission data are sensitive to internal ice shelf physical properties to depths of hundreds of meter, although questions remain regarding the impacts of accreted marine ice and crevasses. Modeled emission spectra from 0.4 to 2.5 GHz indicate that additional information on the relative contributions from differing depths can be retrieved, including the ice physical temperature and the properties of near-basal ice. The results motivate continued analyses of these effects to develop future ice shelf sensing methods, in particular the retrieval of the vertical temperature profile, and the preparation of experimental campaigns essential to support these studies.

REFERENCES

[1] S. Wang et al., "Controls on Larsen C ice shelf retreat from a 60-year satellite data record," *J. Geophys. Res., Earth Surf.*, vol. 127, no. 3, Mar. 2022, Art. no. e2021JF006346, doi: 10.1029/2021jf006346.

[2] D. Pollard, R. M. DeConto, and R. B. Alley, "Potential Antarctic ice sheet retreat driven by hydrofracturing and ice cliff failure," *Earth Planet. Sci. Lett.*, vol. 412, pp. 112–121, Feb. 2015.

[3] I. Das et al., "Multidecadal basal melt rates and structure of the Ross ice shelf, Antarctica, using airborne ice penetrating radar," *J. Geophys. Res., Earth Surf.*, vol. 125, no. 3, Mar. 2020, Art. no. e2019JF005241, doi: 10.1029/2019jf005241.

[4] C. R. Bentley and K. C. Jezek, "RISS, RISP and RIGGS: Post-IGY glaciological investigations of the Ross ice shelfin the U.S. programme," *J. Roy. Soc. New Zealand*, vol. 11, no. 4, pp. 355–372, Dec. 1981.

[5] J. W. Clough and B. L. Hansen, "The Ross ice shelf project," *Science*, vol. 203, no. 4379, pp. 433–434, Feb. 1979, doi: 10.1126/science.203.4379.433.

[6] J. D. Robertson and C. R. Bentley, "Seismic studies on the grid western half of the ross ice shelf: RIGGS I and RIGGS II," in *The Ross Ice Shelf: Glaciology and Geophysics*, C. R. Bentley and D. E. Hayes, Eds. 1990. [Online]. Available: https://agupubs.onlinelibrary.wiley.com/action/showCitFormats?doi=10.1029%2FAR042p0055, doi: 10.1029/AR042p0055.

[7] R. H. Ragle, B. L. Hansen, and W. Patenaude, "Deep core drilling in the Ross ice shelf, little America V, Antarctica," U.S. Army Snow Ice Permafrost Res. Establishment, Wilmette, IL, USA, Tech. Rep. 70, 1960.

[8] M. Morlighem et al., "Deep glacial troughs and stabilizing ridges unveiled beneath the margins of the Antarctic ice sheet," *Nature Geosci.*, vol. 13, no. 2, pp. 132–137, Feb. 2020, doi: 10.1038/s41561-019-0510-8.

[9] M. Morlighem, "Measures BedMachine Antarctica, version 3 [data set]," NASA Nat. Snow Ice Data Center Distrib. Active Arch. Center, Boulder, CO, USA, Tech. Rep., 2022, Accessed: Oct. 10, 2023. [Online]. Available: https://nsidc.org/data/nsidc-0756/versions/3, doi: 10.5067/FPSU0V1MWUB6.

[10] G. Macelloni, M. Leduc-Leballeur, F. Montomoli, M. Brogioni, C. Ritz, and G. Picard, "On the retrieval of internal temperature of Antarctica ice sheet by using SMOS observations," *Remote Sens. Environ.*, vol. 233, Nov. 2019, Art. no. 111405, doi: 10.1016/j.rse.2019.111405.

[11] C. Yardim et al., "Greenland ice sheet subsurface temperature estimation using ultrawideband microwave radiometry," *IEEE Trans. Geosci. Remote Sens.*, vol. 60, 2022, Art. no. 4300312, doi: 10.1109/TGRS.2020.3043954.

[12] K. C. Jezek, C. Yardim, J. T. Johnson, G. Macelloni, and M. Brogioni, "Analysis of ice-sheet temperature profiles from low-frequency airborne remote sensing," *J. Glaciology*, vol. 68, no. 271, pp. 1–11, Mar. 2022, doi: 10.1017/jog.2022.19.

[13] M. J. Andrews et al., "The ultrawideband software-defined microwave radiometer: Instrument description and initial campaign results," *IEEE Trans. Geosci. Remote Sens.*, vol. 56, no. 10, pp. 5923–5935, Oct. 2018, doi: 10.1109/TGRS.2018.2828604.

[14] M. Brogioni et al., "Ice sheet and sea ice ultrawideband microwave radiometric airborne eXperiment (ISSIUMAX) in Antarctica: First results from Terra Nova bay," *Cryosphere*, vol. 17, no. 1, pp. 255–278, Jan. 2023, doi: 10.5194/tc-17-255-2023.

[15] K. C. Jezek et al., "Relationships between L-band brightness temperature, backscatter, and physical properties of the Ross ice shelf Antarctica," *IEEE Trans. Geosci. Remote Sens.*, vol. 60, 2022, Art. no. 4306514, doi: 10.1109/TGRS.2022.3218538.

[16] G. Macelloni et al., "Cryorad: A low frequency wideband radiometer mission for the study of the cryosphere," in *Proc. IGARSS*, 2018, pp. 1998–2000, doi: 10.1109/IGARSS.2018.8519172.

[17] M. Andrews, J. Johnson, M. McLinden, and S. Misra, "A study of front end architectures for the PolarRad 0.5–2 GHZ microwave radiometer," in *Proc. IEEE Int. Geosci. Remote Sens. Symp. IGARSS*, Jul. 2021, pp. 7982–7983, doi: 10.1109/IGARSS47720.2021.9554508.

[18] E. Rignot, S. Jacobs, J. Mouginot, and B. Scheuchl, "Ice-shelf melting around Antarctica," *Science*, vol. 341, no. 6143, pp. 266–270, Jul. 2013, doi: 10.1126/science.1235798.

[19] I. A. Zotikov, V. S. Zagorodnov, and J. V. Raikovsky, "Core drilling through the Ross ice shelf (Antarctica) confirmed basal freezing," *Science*, vol. 207, no. 4438, pp. 1463–1465, Mar. 1980, doi: 10.1126/science.207.4438.1463.

[20] J. F. Kirchner and C. R. Bentley, "RIGGS III: seismic short-refraction studies using an analytical curve-fitting technique," in *The Ross Ice Shelf: Glaciology and Geophysics*, C. R. Bentley and D. E. Hayes, Eds., 1990. [Online]. Available: https://agupubs.onlinelibrary.wiley.com/action/showCitFormats?doi=10.1029%2FAR042p0109, doi: 10.1029/AR042p0109.

[21] M. M. Herron and C. C. Langway, "Firn densification: An empirical model," *J. Glaciol.*, vol. 25, no. 93, pp. 373–385, 1980. [Online]. Available: https://www.cambridge.org/core/journals/journal-of-glaciology/article/firn-densification-an-empirical-model/C9A2B038004A938670B689A6DAE6D89E, doi: 10.3189/S0022143000015239.

[22] K. C. Jezek, C. R. Bentley, and J. W. Clough, "Electromagnetic sounding of bottom crevasses on the Ross ice shelf, Antarctica," *J. Glaciology*, vol. 24, no. 90, pp. 321–330, 1979, doi: 10.3189/s0022143000014842.

[23] H. Wexler, "Heating and melting of floating ice shelves," *J. Glaciology*, vol. 3, no. 27, pp. 626–645, 1960, doi: 10.3189/s0022143000023741.

[24] A. P. Crary, "Glaciological regime at little America station, Antarctica," *J. Geophys. Res.*, vol. 66, no. 3, pp. 871–878, Mar. 1961.

[25] M. Brogioni, G. Macelloni, F. Montomoli, and K. C. Jezek, "Simulating multifrequency ground-based radiometric measurements at dome C—Antarctica," *IEEE J. Sel. Topics Appl. Earth Observ. Remote Sens.*, vol. 8, no. 9, pp. 4405–4417, Sep. 2015, doi: 10.1109/JSTARS.2015.2427512.

[26] L. Tsang and J. A. Kong, *Scattering of Electromagnetic Waves: Advanced Topics*. Hoboken, NJ, USA: Wiley, 2001.

[27] G. Picard et al., "Simulation of the microwave emission of multi-layered snowpacks using the dense media radiative transfer theory: The DMRT-ML model," *Geoscientific Model Develop.*, vol. 6, no. 4, pp. 1061–1078, Jul. 2013, doi: 10.5194/gmd-6-1061-2013.

[28] R. D. West, D. P. Winebrenner, L. Tsang, and H. Rott, "Microwave emission from density-stratified Antarctic firn at 6 cm wavelength," *J. Glaciology*, vol. 42, no. 140, pp. 63–76, 1996.

[29] H. B. Clausen et al., "Surface accumulation on the Ross ice shelf," *Antarct. J. US*, vol. 5, no. 5, pp. 68–72, 1979.

[30] C. Mätzler, "Microwave dielectric properties of ice," in *Thermal Microwave Radiation: Applications for Remote Sensing* (IET Electromagnetic Waves Series), vol. 52. 2006, ch. 5, pp. 427–506. [Online]. Available: https://digital-library.theiet.org/content/books/ew/pbew052e, doi: 10.1049/PBEW052E.

[31] M. R. Vant, R. O. Ramseier, and V. Makios, "The complex-dielectric constant of sea ice at frequencies in the range 0.1–40 GHz," *J. Appl. Phys.*, vol. 49, no. 3, pp. 1264–1280, Mar. 1978, doi: 10.1063/1.325018.

[32] M. J. Brodzik, D. G. Long, and M. A. Hardman, "SMAP radiometer twice-daily rSIR-enhanced EASE-grid 2.0 brightness temperatures, version 2 [data set]," NASA Nat. Snow Ice Data Center Distrib. Act. Archive Center, Boulder, CO, USA, 2021, Accessed: Dec. 15, 2023. [Online]. Available: https://nsidc.org/data/nsidc-0738/versions/2, doi: 10.5067/YAMX52BXFL10.

[33] D. G. Long, M. J. Brodzik, and M. Hardman, "Evaluating the effective resolution of enhanced resolution SMAP brightness temperature image products," *Frontiers Remote Sens.*, vol. 4, Mar. 2023, Art. no. 1073765, doi: 10.3389/frsen.2023.1073765.

[34] Y. H. Kerr et al., "The SMOS mission: New tool for monitoring key elements of the global water cycle," *Proc. IEEE*, vol. 98, no. 5, pp. 666–687, May 2010, doi: 10.1109/JPROC.2010.2043032.

[35] E. Njoku and D. Entekhabi, "Passive microwave remote sensing of soil moisture," *J. Hydrol.*, vol. 184, nos. 1–2, pp. 101–129, Oct. 1996, doi: 10.1016/0022-1694(95)02970-2.

[36] H. Xu et al., "Polar firn properties in Greenland and Antarctica and related effects on microwave brightness temperatures," *Cryosphere*, vol. 17, no. 7, pp. 2793–2809, Jul. 2023.

Open Access funding provided by 'Consiglio Nazionale delle Ricerche-CARI-CARE-ITALY' within the CRUI CARE Agreement